DD2365 - Advanced Computation in Fluid Mechanics

Project: Thermal mixing in T-junctions

Report

Aurélien Coussat – coussat@kth.se
Ezhilmathi Krishnasamy – kriezh@kth.se
Mattia Bergagio – bergagio@kth.se

May 27, 2017

1 Background

Thermal mixing appears to be of great importance in a large variety of engineering and biological fields. For instance, this phenomenon is largely studied in nuclear power plants, where the efficiency of cooling systems is critical.

We decided to conduct the study on a T-junction. One main stream of hot liquid flows in a large pipe, while a smaller, 90-degrees inclined pipe creates an influx of coolant which is mixed to the warmer fluid. We then studied how the two fluids of different temperature mix.

The ultimate goal is to reduce thermal fatigue. A reduced thermal fatigue implies an elongated lifespan for the pipe, which is obviously a desired effect in nuclear power plants. Several techniques can be employed to reduce thermal fatigue, such as the modification of the geometry of the pipe.

Several papers have already been published on the topic at hand, including both analytical and experimental endeavors (for instance, Fukushima et al. [2003]), but it is hard to find data on what we are trying to simulate, that is *thermal mixing in a ninety-degree T-junction with laminar inlets*. The reason is that, in real-life scenarios, flows tend to be turbulent. Hence, 2D cases mainly investigate laminar flows.

For the 3D case, we focused on Kamide et al. [2009], where different velocities at the inlets of a T-junction were studied. The inlets had different diameters as well. The simulations in the above article were run using the Finite Volume Method. Each simulation stemmed from different boundary conditions. However, we took only one case, which is compared qualitatively against our simulation using FEM (FEniCS-HPC).

2 Research question

The following cases are considered:

1. Case 1: 2D model, flat profile at the inlets, free-slip condition at the walls (that is, $\mathbf{u} \cdot \mathbf{n} = 0$), energy equation, Robin boundary condition at the walls (that is, $-k \nabla T \cdot \mathbf{n} = h (T - T_b)$).

2. Case 2: 2D model, parabolic profile at the inlets, no-slip condition at the walls (that is, $\mathbf{u} = \mathbf{0}$), energy equation, Robin boundary condition at the walls.

3. Study of stabilization parameter on a 2D case.

4. Case 3: 3D model, flat profile at the inlets, and free-slip boundary condition at the walls.

5. Validation of the 3D model against experiments.

3 Method

Continuity equation for incompressible flow:

$$\nabla \cdot \mathbf{u} = 0 \,. \tag{1}$$

Incompressible Navier-Stokes momentum equation:

$$\frac{\partial \mathbf{u}}{\partial t} + \mathbf{u} \cdot \nabla \mathbf{u} = -\frac{1}{\rho} \nabla p + \nu \nabla^2 \mathbf{u} + \mathbf{g} \,. \tag{2}$$

Here, gravity field $\mathbf{g}$ is neglected.
The corresponding boundary conditions read as follows:

$$\begin{cases} \mathbf{u} \text{ set at the inlets} \\ p = 0 \text{ at the outlet} \\ \mathbf{u}|_{t=0} = \mathbf{0} \text{ inside the domain.} \end{cases} \tag{3}$$

Case-dependent boundary conditions are not mentioned here.
The energy equation and the corresponding boundary conditions are as follows:

$$\begin{cases} \frac{\partial T}{\partial t} + \mathbf{u} \cdot \nabla T = \alpha \nabla^2 T \\ -k \nabla T \cdot \mathbf{n} = h \left(T - T_b \right) \text{ at the walls} \\ T \text{ set at the inlets} \\ \nabla T \cdot \mathbf{n} = 0 \text{ at the outlet} \\ T|_{t=0} = T_b \text{ inside the domain.} \end{cases} \tag{4}$$

Temperature is treated as a passive scalar.
Coefficients h, T_b, α and ν, together with T and $\mathbf{u}$ at the inlets, can be easily found in our Python scripts for Cases 1 and 2.
The cG(1)cG(1) method leads to the following weak formulation of Eqs. (1) and (2):

$$\begin{aligned} &\left(\left(U^n - U^{n-1} \right) k_n^{-1} + \nabla P^n + \bar{U}^n \cdot \nabla \bar{U}^n, v \right) + \left(\nu \nabla \bar{U}^n, \nabla v \right) + \\ &\left(\nabla \cdot \bar{U}^n, q \right) + SD_\delta^n \left(\bar{U}^n, P; v, q \right) = 0 \,. \end{aligned} \tag{5}$$

Here, k_n is the time step, $\bar{U}^n$ is calculated as

$$\bar{U}^n = \frac{1}{2} \left(U^n + U^{n-1} \right) \,, \tag{6}$$

while the stabilization term is expressed as

$$SD_\delta^n \left(\bar{U}^n, P; v, q \right) = \left(\delta_1 \left(\bar{U}^n \cdot \nabla \bar{U}^n + \nabla P^n \right), \bar{U}^n \cdot \nabla v + \nabla q \right) + \left(\delta_2 \nabla \cdot \bar{U}^n, \nabla \cdot v \right) \,, \tag{7}$$

where stabilization parameters δ_1 and δ_2 read

$$\delta_1 = \kappa_1 \left(k_n^{-2} + \left| U^{n-1} \right|^2 h_n^{-2} \right)^{-1/2} \tag{8}$$

and

$$\delta_2 = \kappa_2 \, h_n \,, \tag{9}$$

respectively (Hoffman et al. [2015]). h_n is the mesh size.
The weak formulation of Eq. (4) can be written as

$$\begin{aligned} &\left((T^n - T^{n-1}) \, k_n^{-1} + \bar{U}^n \cdot \nabla \bar{T}^n, z \right) + \left(\left(\alpha + \delta_3 \, k_n^{-1} \right) \nabla \bar{T}^n, \nabla z \right) + \\ &\frac{h}{\rho \, c_p} \int_{S_{wall}} \left(T^n - T_b \right) z \, dS = 0 \,, \end{aligned} \tag{10}$$

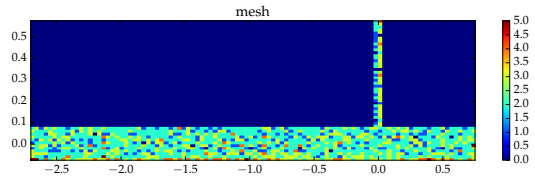

(a) Adaptive refinement 0.

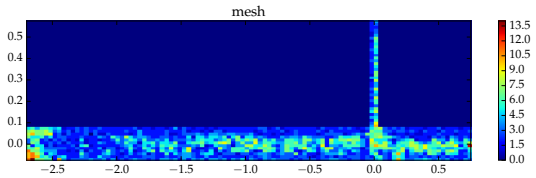

(b) Adaptive refinement 1.

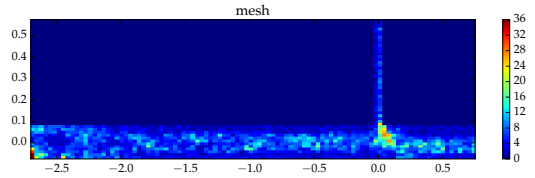

(c) Adaptive refinement 2.

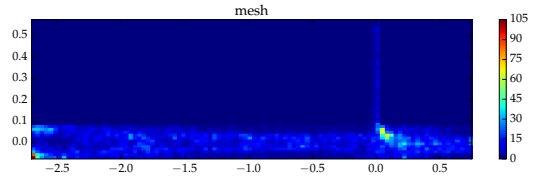

(d) Adaptive refinement 3.

Figure 1: Left: Mesh points for Case 1.

where stabilization parameter δ_3 reads

$$\delta_3 = 1 \times 10^{-5} \frac{h_n}{|U^n|} \,. \tag{11}$$

The linearized adjoint equations

$$-\dot{\phi} - u \cdot \nabla\phi + \nabla U^T \phi + \nabla\theta = \psi \tag{12}$$

and

$$\nabla \cdot \phi = \chi \tag{13}$$

were solved with respect to θ and ϕ after setting $\phi(\cdot, T) = 0$, T being the last simulation time. Coefficients ϕ and χ can be easily found in our Python scripts for Cases 1 and 2. Here we used the approximation $u \approx U$.
The corresponding stabilization term is written as

$$\begin{aligned} SD_\delta\left(U, \theta, \phi, \psi; v, q\right) \approx & \left(\delta_3 \left(-U \cdot \nabla\phi + \nabla U^T \phi + \nabla\theta - \psi\right), -U \cdot \nabla v + \nabla U^T v + \nabla q\right) + \\ & \left(\delta_4 \nabla \cdot \phi, \nabla \cdot v\right) \,. \end{aligned} \tag{14}$$

4 Results

4.1 Case 1

The mesh was refined based on the velocity along the x-axis – see Fig. 1. Videos are available here.

4.2 Case 2

See Figs. 2 and 3. Videos are available here.

4.3 Study of stabilization parameter on a 2D case

Case 2, old: two outlets, parabolic profile at both the inlet and the branch outlet, no-slip condition at the walls, energy equation, Robin boundary condition at the walls. See Figs. 4, 5, and 6.

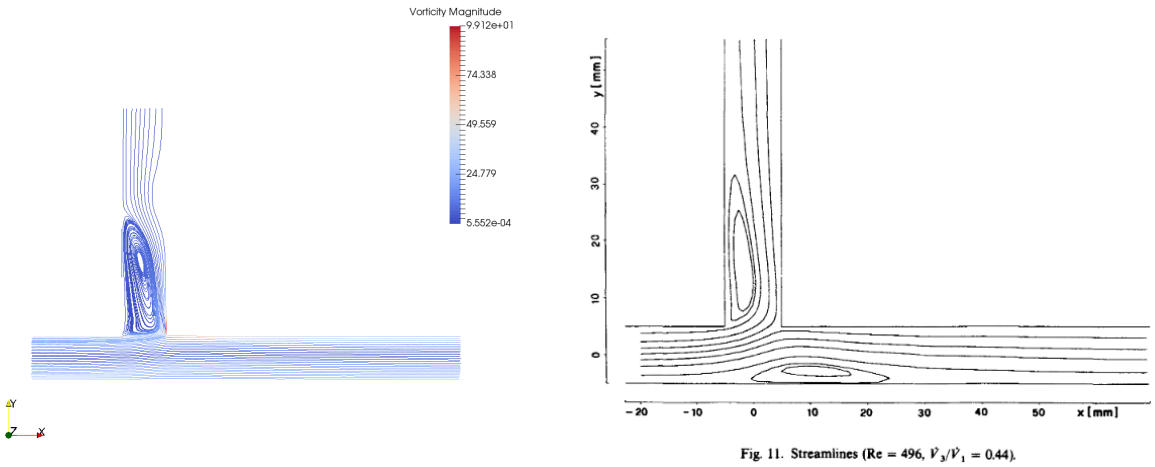

Fig. 11. Streamlines (Re = 496, $V_3/V_1 = 0.44$).

Figure 2: Left: Streamlines for Case 2 at time $t \approx 10\,\mathrm{s}$. Refinement iteration no. 3. Goal functional based on the velocity along the x-axis.
Right: Validation against Liepsch et al. [1982].

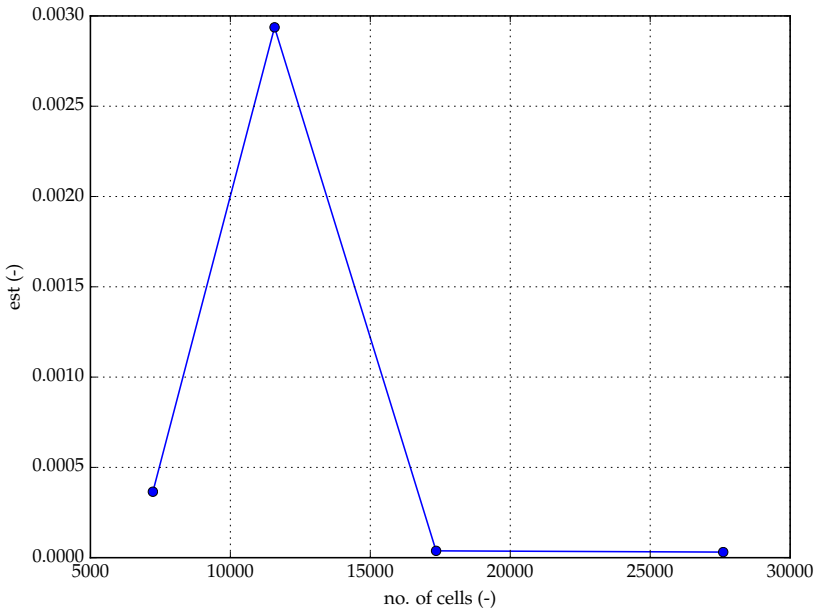

Figure 3: Error estimate towards a goal functional based on the velocity along the x-axis. The refinement ratio equals 0.1. No more than four iterations.

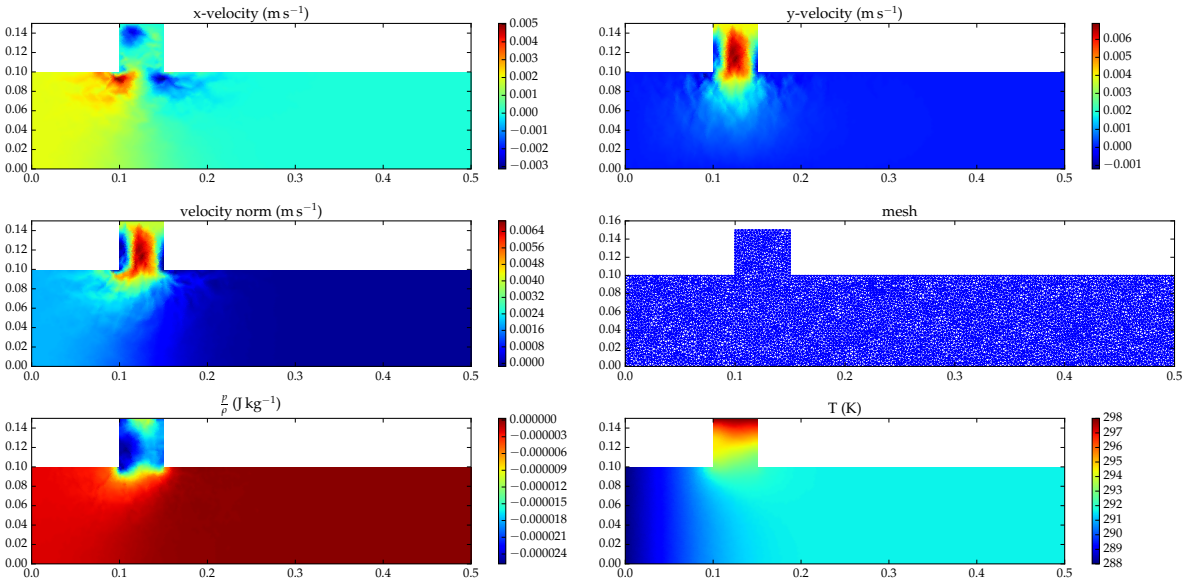

Figure 4: $\mathbf{u}$, p, and T for Case 2, old at time $t \approx 1300\,\mathrm{s}$ with κ_1 and κ_2 equal to 1.

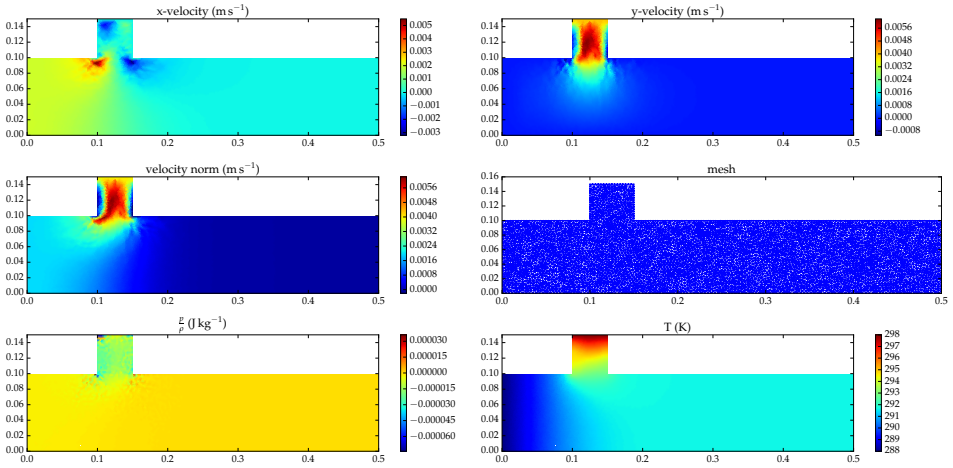

Figure 5: $\mathbf{u}$, p, and T for Case 2, old at time $t \approx 115\,\mathrm{s}$ with κ_1 and κ_2 equal to 0.1.

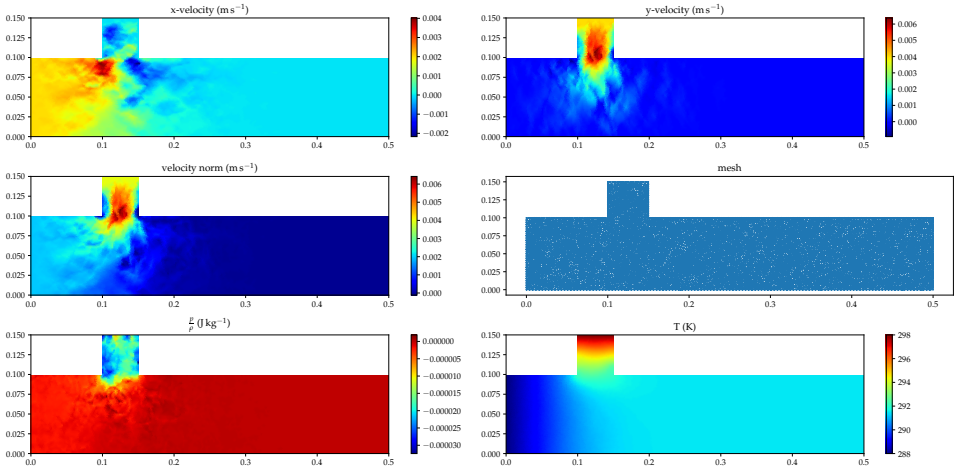

Figure 6: $\mathbf{u}$, p, and T for Case 2, old at time $t \approx 45\,\mathrm{s}$ with κ_1 and κ_2 equal to 10.

5 Discussion

5.1 Case 1

Since turbulence and vortexes are mainly three-dimensional phenomena, Case 1 can only hint at the complexity of the flow field from Case 3. However, the videos suggest that convection might play a major role in the determination of the final temperature profile.

5.2 Case 2

Our simulations can correctly predict the separation bubbles in the two ducts; that is, the larger one in the branch duct and the smaller one downstream of the bifurcation. Corners might be triggering the larger separation bubble. Furthermore, as expected, the streamlines are linearly distributed close to the outlets. Please note that, unlike that from Liepsch et al. [1982], ours is a transient simulation.
Fig. 3 implies that, for a refinement ratio of 0.1, three refinement iterations are enough to reduce the error estimate below the initial value.

5.3 Study of stabilization parameter on a 2D case

The results for Case 2, old with κ_1 and κ_2 equal to 0.1 show some artifacts in the pressure field (see Fig. 5). κ_1 and κ_2 as high as 10 are not needed, since κ_1 and κ_2 equal to 1 can ensure stability (see Fig. 4).

5.4 Case 3

For the 3D case, we have not computed the energy equation (i.e., no heat transfer problem is considered, only the flow problem is considered). And also for the simplicity, we have chosen to have a flat profile inlet velocity and free-slip boundary condition. This makes us to choose the cheaper computation on the walls.

The following boundary condition were set in the simulation: Inlet velocity is $1.46\,\mathrm{m\,s^{-1}}$ for the main pipe and for the branch pipe inlet velocity is $1.00\,\mathrm{m\,s^{-1}}$. The outlet pressure is set to $0\,\mathrm{J\,kg^{-1}}$. Kinematic viscosity is chosen as $1 \times 10^{-6}\,\mathrm{m\,s^{-1}}$ as per the fluid room temperature. The dimension of the main pipe inlet diameter is 0.150 m and branch pipe inlet diameter is 0.075 m. The total length of the main pipe is 1 1 m. 3D simulation computed in the Beskow super computer at KTH-PDC, 5 nodes of 160 cores were chosen with total 5 hours. We were able to ran up to 6 adaptivity iterations with 5 % adaptivity setup.

Table 1 shows the number of elements after each adaptivity iteration. Here the adaptivity is based on the mean velocity along the x-axis. This can be seen in Figure 7

5.5 Validation - 3D flow mixing

Figures 8 and 9 show the vortex streamlines are almost identical to each other. This comparison is based on the experimental results. Based on different velocities, they have categorized flow patterns as three, they are: wall jet, deflecting jet and impinging jet. But we only did the simulation against the wall jet approach (which has main branch pipe velocity is greater than the branch pipe velocity). Figure 10 shows the glyph is

Adaptivity iteration	No. of nodes
0	70 791
1	94 738
2	120 908
3	154 230
4	201 299
5	264 503
6	350 217

Table 1: Adaptivity iteration

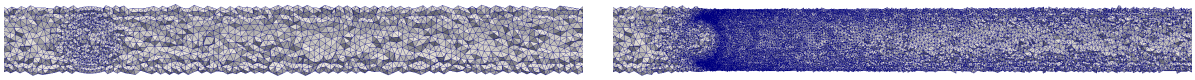

Figure 7: Left: Mesh at adaptive refinement iteration no. 0 (number of nodes = 350217). Right: Mesh at adaptive refinement iteration no. 7 (number of nodes = 4647704). Refinement ratio equal to 0.05. Mesh adaptivity is shown here at $y = 0.065\,\mathrm{m}$.

compared with streamline. This also shows the flow pattern and vortex formation is almost identical to each other.

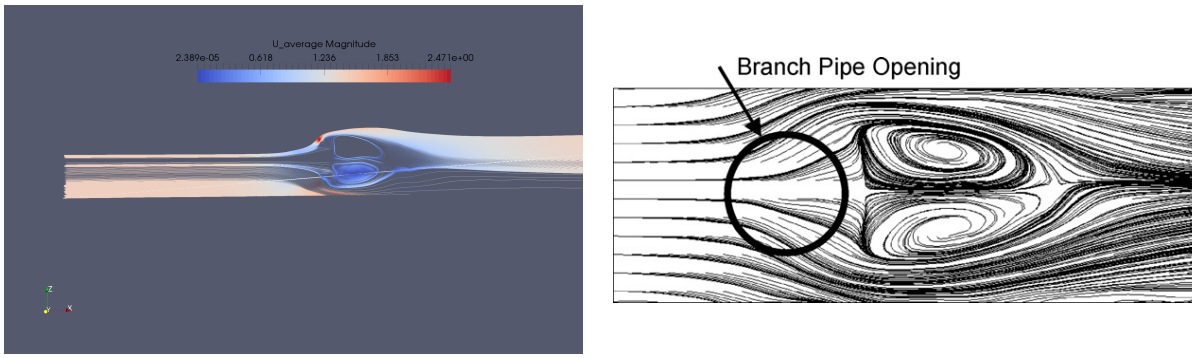

Figure 8: Time-averaged streamlines on plane $y = 65\,\mathrm{mm}$.
Left: Bottom vortex. Our simulation. Right: Vortexes from Kamide et al. [2009].

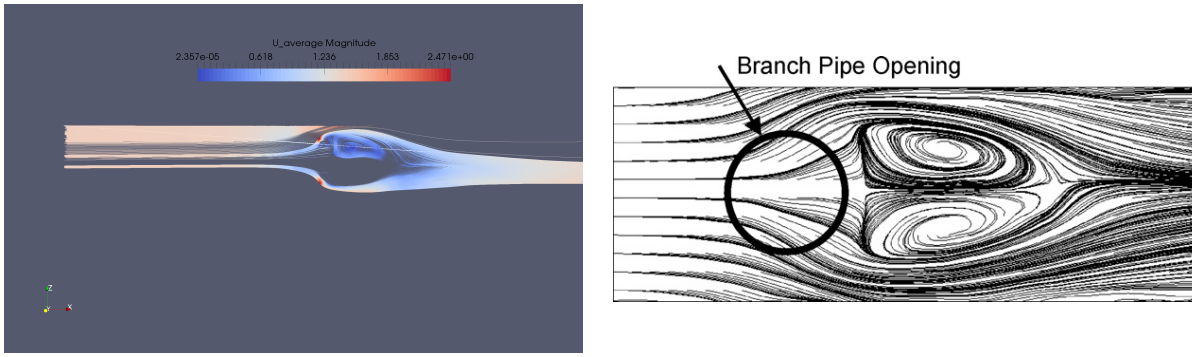

Figure 9: Time-averaged streamlines on plane $y = 65\,\mathrm{mm}$.
Left: Top vortex. Our simulation. Right: Vortexes from Kamide et al. [2009].

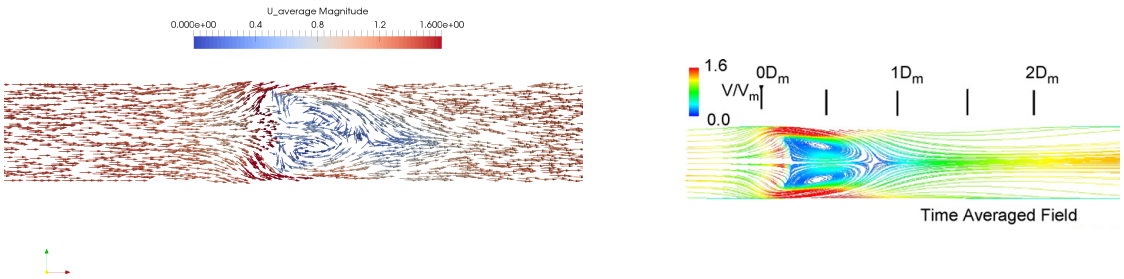

Figure 10: Left: Time-averaged glyphs on plane $y = 65\,\mathrm{mm}$. Our simulation.
Right: Streamlines from Kamide et al. [2009].

References

N. Fukushima, K. Fukagata, N. Kasagi, H. Noguchi, and K. Tanimoto. Numerical and experimental study on turbulent thermal mixing in a t-junction flow. 2003(6):249, 2003. URL `http://ci.nii.ac.jp/naid/110002495656/en/`.

J. Hoffman, J. Jansson, N. Jansson, and R.V. De Abreu. Towards a parameter-free method for high Reynolds number turbulent flow simulation based on adaptive finite element approximation. *Computer Methods in Applied Mechanics and Engineering*, 288:60–74, 2015.

H. Kamide, M. Igarashi, S. Kawashima, N. Kimura, and K. Hayashi. Study on mixing behavior in a tee piping and numerical analyses for evaluation of thermal striping. *Nuclear Engineering and Design*, 239(1):58–67, 2009.

D. Liepsch, S. Moravec, A.K. Rastogi, and N.S. Vlachos. Measurement and calculations of laminar flow in a ninety degree bifurcation. *Journal of Biomechanics*, 15(7):473 – 485, 1982. ISSN 0021-9290. doi: http://dx.doi.org/10.1016/0021-9290(82)90001-X.

A Videos

Link to videos for Cases 1, 2, and 3